BOND GRAPH MODELING OF REVERSE-FLOW MONOLITH REACTOR FOR AIR POLLUTANT ABATEMENT

A. Riaud [(a)], S. Paul [(a,b,c)], G. Dauphin-Tanguy [(a,b,d)]

[(a)] Ecole Centrale de Lille, F-59651 Villeneuve d'Ascq Cedex, France.
[(b)] Univ. Lille Nord de France, F-59000, Lille, France.
[(c)] CNRS UMR8181, UCCS, F-59655 Villeneuve d'Ascq Cedex, France.
[(d)] CNRS FRE 3303, LAGIS, Ecole Centrale de Lille, F-59651 Villeneuve d'Ascq Cedex, France.

[(a)]antoine.riaud@centraliens-lille.org, [(b)]sebastien.paul@ec-lille.fr, [(c)]genevieve.dauphin-tanguy@ec-lille.fr

ABSTRACT
A bond graph model of a reverse-flow monolith reactor has been developed. It aims at offering a tool for the design of such devices, optimizing control strategies and generating code for this control. The construction of the model is detailed and compared with previous results issued from the literature. The influence of some driving parameters on the dynamic behavior of the system and the pollutant abatement is discussed from simulation results.

Keywords: bond-graph, reverse-flow monolith reactor, combustion, VOC, pollutant abatement

1. INTRODUCTION
The Volatile Organic Compounds (VOC) emission in the atmosphere by industrial processes (as for instance by a painting workshop of the car industry) is currently a major environmental issue. As a matter of fact, these compounds cause respiratory disorders, greenhouse effect and are even sometimes carcinogens. Therefore, highly efficient low cost solutions need to be implemented for the abatement of these air pollutants. The most attractive end-of-the-pipe treatments involve thermal or catalytic oxidation of these compounds. In the latter case the use of a solid catalyst allows working in the continuous mode at relatively moderate temperature. However, even if total oxidation reactions are exothermic, conventional combustion reactors are energy demanding particularly in the case of the treatment of highly diluted effluents. Therefore energy consumption has to be reduced by recovering the heat released during combustion (process integration). Reverse-Flow Reactors (RFR) have proved to be efficient in such a case even if the dilution of the VOC is high and if the temperature of the feed is low (Van de Beld and Westerterp 1994a, Van de Beld et al 1994b). To decrease the pressure drop induced by the catalytic bed, monolithic support with a so-called honeycomb structure which walls are coated with the catalyst are often used to pack this kind of reactor (Matros and Bunimovich 1996). Basically, the RFR is a fixed-bed reactor where the direction of the feed is alternatively switched from one way to another. In this case the heat of the reaction is partially stored in the monolith and then restored to heat the feed to be treated. When the pseudo steady-state is reached the RFR is sometimes capable to work auto-thermally, which is, of course, the most efficient way to carry out pollutants abatement.
Obviously, the temperature and the concentrations profiles inside the reactor change continually because of the intrinsic unsteady-state of this process. To calculate these profiles, RFR are generally modeled by a set of differential-algebraic equations corresponding to the non-stationary mass and energy balances (Marin et al 2009). In the present work, a Bond Graph modeling of such a process is developed in order to study the influence of the switching time on transient and pseudo steady-state reactor behavior.

Some publications concern the study of the physical parameters behavior inside such a reverse-flow reactor using detailed models. For instance, Balcaen (2011) used a 2D model to calculate temperature and pollutant distribution in the reactor. Ramdani et al (2001) developed a linear control model for short switching periods reactors (with a very small catalytic zone). However, because they are time-consuming and often too restrictive, none of these models open prospects to integrate the reactor in the overall plant design (pumps, pipes, power supply...), and to adapt control strategies during the development.

The bond graph language can bring a solution because it allows the coupling of several physical fields, simplifies the study of non-linear systems, automatically finds system variables, is easy to simplify or to make more accurate, and, through the physics, suggests sizing optimization and control strategies.
Some papers in the literature deal with bond graph models of chemical reactors such as continuously stirred tank reactors (Heny et al 1999), perfectly mixed gas autoclaves and membranes (Couenne et al 2006), batteries (Karnopp 1990, MacKenzie et al 1993, Thoma and Ould-Bouamama 1999) but, as far as we know, none of them concern directly a reverse-flow reactor.

This paper is organized as follows. After this short introduction, the second section deals with the description of the general structure of the reverse-flow reactor and the definition of the model. In the third section, after defining the variables used for the modeling in pseudo-bond graph (BG), and the chosen hypotheses, two BG models of a once-through reactor are described with an increasing complexity. In the fourth section, it is shown how to extend this model to the reverse-flow reactor. Some comparisons are made using literature results in the fifth section. Thus the model is used to study the influence on the efficiency of air pollutant abatement of some parameters as for instance the semi-cycle time, the dynamic variation of the pollutant inlet concentration and the reactor start-up.

2. REVERSE-FLOW REACTOR DESCRIPTION

2.1. Structure of the RFR

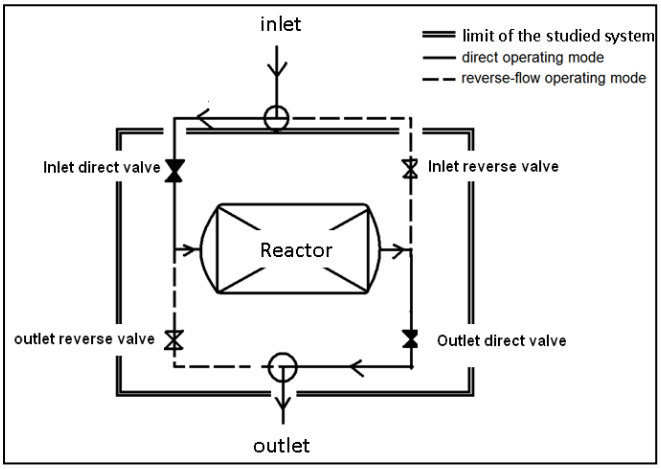

Figure 1: General Description of a Reverse-Flow Reactor

Figure 1 gives a general description of a RFR. This reactor is packed with a monolith whose walls are coated with an appropriate combustion catalyst. In the first semi-cycle the polluted air is introduced to the left and if the temperature reached on the catalyst surface is sufficient the reaction of combustion occurs. The heat released is then partly evacuated by the downstream gas and partly stocked in the monolith. Then in the second half-cycle the direction of circulation of the gas is inverted. The heat stocked in the monolith is then used to heat-up the cold polluted air entering the reactor at the right side this time.

The studied reactor is made of several tubular channels. As shown in Figure 2, each channel is composed of four layers: the polluted air in the middle, the washcoat and catalyst layers, the monolith by itself and finally an equivalent virtual insulation coating modeling the real insulation coating around the overall reactor as shown in equation (50).

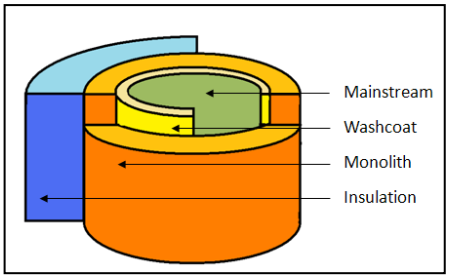

Figure 2: Cross-Section of a Single Channel of the Reactor

The proposed model represents only one channel but can be easily extended to the whole monolith. Pollutants are transported through the channel, and burn on the catalyst's surface. A part of the heat generated is released in the air, and another part is stocked in the monolith.
Air flow direction is periodically inverted; half-period is called the semi-cycle time.

2.2. Model Assumptions

For simulation purpose, the channel is axially subdivided in n cells. In the cells, the following assumptions are made:

- The temperature, pressure and composition are axially uniform
- The gas phase is considered as ideal (low pressure)
- No mass-transfer occurs from the catalyst to the monolith (airtight material)
- The combustion is a first-order reaction and follows the Arrhenius law (Ramanathan 2004)
- Each channel in a cross-section of the reactor has the same thermal profile
- Axial mass and heat transfer within the washcoat are neglected
- Axial diffusive heat and mass transfer within the channel are neglected (compared to convective heat and mass transfer)
- Thermal capacities are non-temperature-dependent
- The gas phase is only composed of O_2, N_2, propane C_3H_8 (considered as a model molecule for the pollutant), CO_2 and H_2O.
- The combustion enthalpy is non-temperature-dependent (Kirchhoff law validates this hypothesis within 1% in the considered temperature range).
- Inertial phenomena are neglected compared to pressure phenomena (Re << 2300)
- The data provided for modeling are inlet gas mass flow rate $q_{m,in}$, the inlet temperature T_{in}, the ambient air temperature T_{atm} and the inlet molar fraction x_i of each component i.
- The diameter of the channel is much smaller than the length of the reactor so the entrance

effect of fluid mechanics are neglected (Nu, Sh = Nu_∞, Sh_∞)

3. MODEL CONSTRUCTION IN CASE OF SINGLE MONO-DIRECTIONAL FLOW

3.1. Choice of Variables

Previous works in this field have shown that equations are simpler when written with molar flow rates, partial pressures, heat flow rates or enthalpy flow rates and temperature. Therefore, the proposed model is built using these variables, it is hence a pseudo-bond graph. Three types of power bonds are used:

Table 1: Bonds and state variables of the bond graph model

Field	Mass Transfer (Gas Variable Composition)	Mass Transfer (Mixture, variable Composition)	Heat Transfer (Convective)	Heat Transfer (Conducive)
Symbol				
Flow	$\dot{n}$	$\dot{n}_i$	$\dot{H}$	$\dot{Q}$
Effort	P	P_i	T	T

The mass transfer multi-bonds carries one flow for each chemical species.

3.2. Three Cells Model

In a first step, a simple mono-directional flow is modeled. Several material layers storing matter and heat are represented by multiport C elements. Some pressure drop and convection heat transfer occurring between the layers are represented using multiport R elements.

If the feed gas has a temperature lower than the washcoat, then a heat transfer will occur upstream and the air will get hotter. Then, in the second cell, the combustion can start if the gas is hot enough. The products are released in the same cell because we assume no convection occurs close to the walls. The reaction is exothermal and a part of the heat generated by the combustion is exchanged with the flow. This hot fluid warms-up the downstream cell.

For clarity purpose, the model is presented here with only 3 cells: inlet, combustion and outlet cell. As shown in Figure 3, polluted air is considered as gas with known composition $x_{i\text{-}in}$, mass flow rate $q_{m,in}$ and temperature T_{in}. For the inlet cell, molar flow rate $\dot{n}_{in,i}$ and enthalpy flow rate $\dot{H}_{in}$ are calculated using equations (1) and (2).

$$\dot{n}_{in,i} = \frac{q_{m,in}}{M} x_{i,in} \quad (1)$$

$$\dot{H}_{in} = \frac{q_{m,in}}{M} C_p T_{in} \quad (2)$$

One single bond is used for the outlet pneumatic part, because the mass flow rate does not depend on the atmosphere composition but on the total pressure.

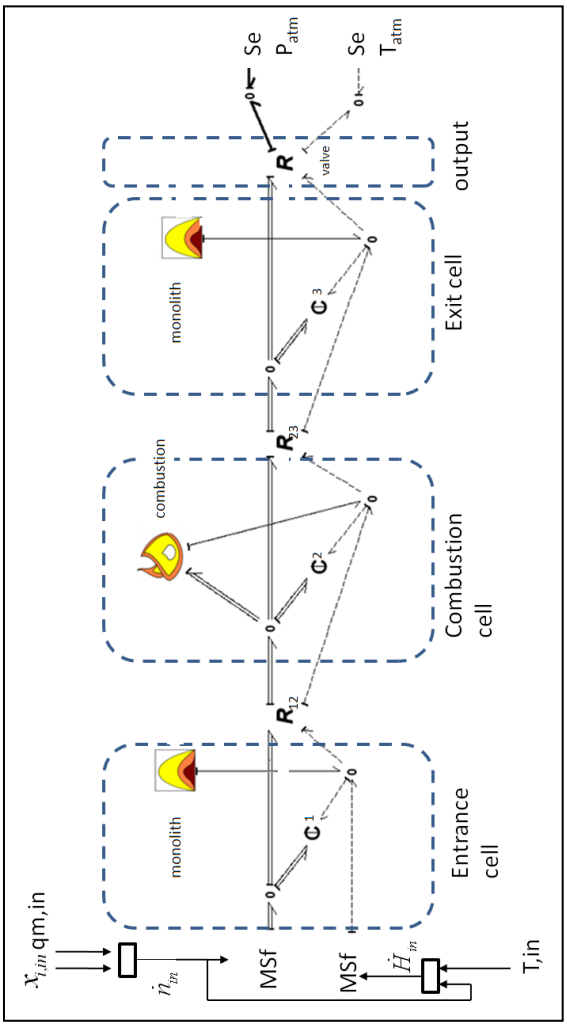

Figure 3: 3 Cells Channel Model

- Equations for the C-elements

Consider for example C2-element.

The number of moles of species i is given by equation (3) coupled with (4) where the different terms correspond to the species molar flow rates through the R-elements and to the combustion zone.

For C1 and C3, no combustion occurs: $\dot{n}_{i_{1\to combustion}} = 0$

$$n_{i_{C2}} = \int \dot{n}_{i_{C2}}\, dt \quad (3)$$

$$\dot{n}_{i_{C2}} = \dot{n}_{i_{1\to 2}} - \dot{n}_{i_{2\to 3}} - \dot{n}_{i_{2\to combustion}} \quad (4)$$

The temperature in each cell i is given by equation (5) coupled with (6) and (7). The different terms in (6) correspond to the convective heat flow rates through the R-elements, the conduction heat flow from the monolith and the combustion heat (only for C2).

$$T_{C2} = \frac{1}{C_{th}} \int \dot{H}_{C2}\, dt \quad (5)$$

$$\dot{H}_{C2} = \dot{H}_{1\to C2} + \dot{Q}_{combustion\to C2} - \dot{H}_{C2\to R23} + \dot{Q}_{monolith} \quad (6)$$

$$C_{th} = nC_p \quad (7)$$

The partial pressures in each cell i are given by equation (8) and the total pressure and total number of moles by equations (9) and (10). The volume of each cell is constant.

$$P_{i_{C2}} = \frac{n_{i_{C2}} RT_{C2}}{V_{cell}} \quad (8)$$

$$P_{C2} = \sum_i P_{i_{C2}} \quad (9)$$

$$n_{C2} = \sum_i n_{i_{C2}} \quad (10)$$

- The reaction block is a kinetic formula which has to link the Gibbs energy with the reaction rate.

The chemical reaction is

$$C_3H_8 + 5O_2 = 4H_2O + 3CO_2 + Q_{combustion}$$

As it was written before, the bond-graph is not restrictive to Arrhenius kinetic model. It was a choice to model the combustion as a first-order reaction.

$$r_v = A_r \exp\left(\frac{-E}{RT_{C2}}\right) \quad (11)$$

$$\dot{n}_{C_3H_8} = r_v \frac{P_{C_3H_8}}{RT_{C2}} V_{cat} \quad (12)$$

Where V_{cat} is the volume of catalyst per cell

$$\dot{n}_{O_2} = 5\dot{n}_{C_3H_8} \quad (13)$$

$$\dot{n}_{H_2O} = -4\dot{n}_{C_3H_8} \quad (14)$$

$$\dot{n}_{CO_2} = -3\dot{n}_{C_3H_8} \quad (15)$$

$$\dot{Q}_{combustion} = -\dot{n}_{C_3H_8}\Delta_r H° \quad (16)$$

- Equations for R-elements

Consider for instance R23-element.

The volume flow rate in R23, given by equation (18), allows the calculation of the different flow rates needed for the C-elements.

$$Q_{v_{2\to3}} = \frac{\pi D^4}{128\mu L_{cell}}(P_{C2} - P_{C3}) \quad (17)$$

$$\dot{n}_{2\to3} = \frac{P_{C2}Q_{v_{2\to3}}}{RT_{C2}} \quad (18)$$

$$\dot{H}_{2\to3} = \dot{n}_{2\to3}C_pT_{C2} \quad (19)$$

$$\mu = \mu_a T_{C2} + \mu_b \quad (20)$$

$$\dot{n}_{i_{2\to3}} = \frac{P_{iC2}}{P_{C2}}\dot{n}_{2\to3} \quad (21)$$

The R-element corresponding to matter and heat transfer to environment is described hereafter.

- Equations for R_{output} (in once-through operating mode, $D_g = D$)

$$Q_{v_{3\to out}} = \frac{\pi {D_g}^4}{128\mu L_g}(P_{C3} - P_{out}) \quad (22)$$

$$\dot{n}_{3\to out} = \frac{P_{C3}Q_{v_{3\to out}}}{RT_{C3}} \quad (23)$$

$$\dot{H}_{3\to out} = \dot{n}_{3\to out}C_pT_{C3} \quad (24)$$

$$\mu = \mu_a T_{C3} + \mu_b \quad (25)$$

At this point, a basic model for once-through operating mode has been built.

This model is extended in the next section by introducing the dynamic of heat transfer between the channel and the monolith.

3.3. Extension of the 3 cells-model

The heat transfer and mass transfer between combustion sub-system and channel sub-system involve a boundary layer. It is a 1D correlation of heat and mass-transfer between the gas and the washcoat, which temperature and composition are supposed to be homogeneous. It is a relevant parameter because during simulation, a thermal gradient of about 10K was calculated within this boundary layer. It is represented by an R-element. Figure 4 shows the detailed and extended model of a cell.

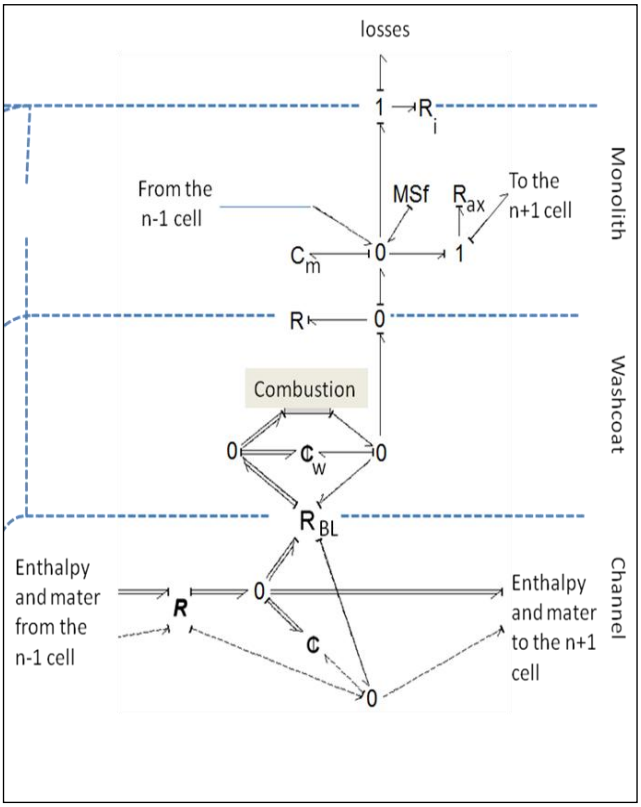

Figure 4: Detailed Bond Graph Model of a Cell

- Equations for the boundary layer R_{BL}

The heat flow rate is calculated using washcoat and mainstream temperatures in (26)

$$\dot{Q}_{BL} = \frac{1}{R_{th}}(T_w - T_{ms}) \quad (26)$$

Where $R_{th} = \frac{1}{\pi hD}$ (27)

With $h = \frac{kNu}{D}$ (28)

For the same reason as viscosity, thermal conductivity and diffusivity were linearly approximated. The temperature was taken in the washcoat capacitive element.

$$k = k_a T_w + k_b \quad (29)$$

The species molar flow rate is given by equation (30)

$$\dot{n}_i = \frac{1}{R_n}\left(P_{i_{ms}} - P_{i_w}\right) \quad (30)$$

Where $R_n = \frac{1}{\pi \beta R T_w D}$ (31)

With $\beta = \frac{\alpha Sh}{D}$ (32)

and $\alpha = \alpha_a T_w + \alpha_b$ (33)

The washcoat layer is the catalytic layer between the monolith and the mainstream. It was previously neglected as far as mass and heat transfer is concerned because it is very thin. Let's now improve the model considering that this material is porous and can store heat in the catalyst or gas in the pores. A C- element is added in the model to take this into accounts.

- Equations for the washcoat heat and matter storage element Cw

$$\dot{Q}_{Cw} = \dot{Q}_{combustion \to w} - \dot{Q}_{BL} - \dot{Q}_{w \to m} \quad (34)$$

$$\dot{n}_{i_{Cw}} = \dot{n}_{i_{ms}} - \dot{n}_{i_{w \to combustion}} \quad (35)$$

The heat capacity of the air is neglected: heat storage occurs only in the catalyst.

$$T_w = \frac{1}{C_{th}} \int \dot{Q}_w \, dt \quad (36)$$

With $\mathrm{C_{th}} = (1-\varepsilon)\rho_c V_w C_c$ (37)

The matter accumulates inside the pores of the catalyst. The partial pressures are given by equations (38) and (39)

$$P_{i,w} = \frac{RT}{\varepsilon V_w} n_{i,w} \quad (38)$$

With $n_{i,w} = \int \dot{n}_{i,w} \, dt$ (39)

When the reactants diffuse inside the catalyst, part of them is consumed. Concentration in the catalyst is not equal to surface concentration as it can be calculated with ideal gas equation. Hence, equation (12) is slightly modified: η factor makes a correlation between the partial pressures of species on the surface of the catalyst and a medium concentration for the reaction rate. According the simulations η is about 0.8.

Using Thiele factor equations (combustion model accuracy improvement), it leads to

$$\dot{n}_{C_3H_8} = \eta r_v \frac{P_{C_3H_8}}{RT_{Cw}} V_{cat} \quad (40)$$

With $\eta = \frac{\tanh(\theta)}{\theta}$ (41)

Where $\theta = t_w \sqrt{\frac{r_v}{D_e}}$ (42)

Most of the heat is stored in the monolith.

- Equations of the monolith (Cm-element)

The temperature in the monolith is given by

$$T_m = \frac{1}{C_{th}} \int \dot{Q}_{Cm} \, dt \quad (43)$$

With $\mathrm{C_{th}} = \rho_m V_m C_m$ (44)

The monolith stores heat, but also exchanges it axially and radially. Equation (45) gives the heat balance of the nth cell:

$$\left[\dot{Q}_{Cm}\right]_n = \left[\dot{Q}_{w \to m}\right]_n + \left[\dot{Q}_{ax}\right]_{n-1 \to n} - \left[\dot{Q}_{ax}\right]_{n \to n+1} - \left[\dot{Q}_{m \to loss}\right]_n \quad (45)$$

The thermal gradient between the washcoat and the monolith was modeled with an R element.

We make the assumption the thermal conductivity of the washcoat is independent of its porosity. It is legitimized because this resistance is not relevant, and does not require a detailed model. Maxwell or Nielsen correlations are often used for porous materials.

$$\left[\dot{Q}_{w \to m}\right]_n = \frac{1}{R_{th}}\left(T_w - T_m\right) \quad (46)$$

With $R_{th} = \frac{\ln\left(1+\frac{2t_w}{D}\right)}{2\pi k_w L_{cell}}$ (47)

thermal resistance for a cylindrical material

The monolith can also exchange heat axially.

$$\left[Q_{ax}\right]_{n \to n+1} = \frac{1}{R_{th,axial}}\left(\left[T_m\right]_n - \left[T_m\right]_{n+1}\right) \quad (48)$$

With $R_{th_{axial}} = \frac{L_{cell}}{S_m k_m}$ (49)

The MSf models a heater which pre-heats the reactor before reaching autothermal state, or warms-up it enough to burn the gas if the pollutant is too much diluted. A small amount of heat can also be exchanged with other channels or with the outside of the reactor. It is the "to the ambient" port.

The ultimate layer is a virtual layer called insulation layer. It is just an R element associated with an effort source Se representing ambient temperature.

- Equations of the insulation coating

The temperature distribution of all the channels of the reactor was assumed to be the same. It means that the heat carried and removed by the air is much higher than the heat loss. As a consequence all the channels have more or less the same contribution to heat loss. These losses can be equally distributed among the

channels. Moreover, with this assumption, the temperature of the wall of every channel is the same.

$$\left[\dot{Q}_{m\to loss}\right]_{1\_channel} = \frac{\left[\dot{Q}_{loss}\right]_{cross-section}}{N_{channels}} = \frac{T_i - T_{atm}}{N_{channels} R_{insulation}} \quad (50)$$

In the simulations, we assume the reactor's cross section to be square:

$$R_{insulation} = \frac{t_i}{4k_i L_{cell}(D+2t_m+2t_w)\sqrt{N_{channels}}} \quad (51)$$

4. REVERSE- FLOW REACTOR MODEL

To get a more precise model, the central section (combustion cell) is duplicated several times to increase the space convergence of the model. Each duplication of the number of cells multiplies by 4 the calculation time (variable step-solver Vode&Adams). After several simulation tests, it appeared that 82 sections model might be a good compromise between precision and computation time.

Using the graphical conventions given in Table 2, Figure 5 shows the reverse flow reactor global model.

Table 2: Graphical Conventions for Direct and Reverse Flows

	Direct or shared bonds		Exclusive to reverse-flow bonds	
Information				
Mass transfer	gas	mixture	gas	mixture
Enthalpy				

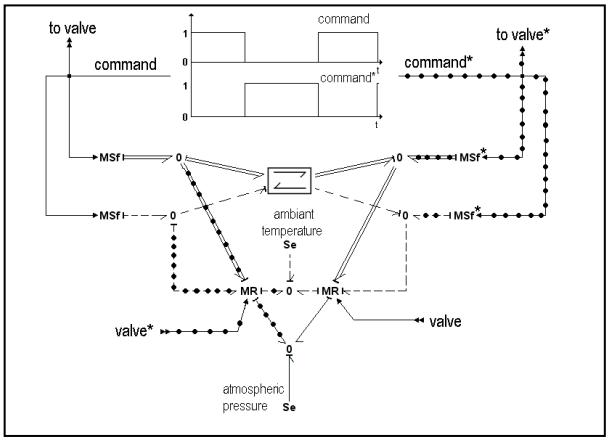

Figure 5: Reverse Flow Reactor Model

For once-through operating mode, the flow is generated by the MSf and "valve" is always opened: the flow follows the continuous bonds. For reverse-flow operating mode, MSf* is added and "gate*" is opened while "gate" is closed and MSf flow generated drops to zero. Hence, the flow in the channel is reversed.

To observe the reverse-flow phenomena, a Boolean was added in the convective heat transfer elements.

The inlet and outlet cells are modified to take into account the reversal of the flow. The inlet flow, modeled with MSf element enters into a C-element, the outlet flow goes out to the environment through a R-element. These R- and C-element have to appear in these cells, but they are used only when needed.

Causality ensuring pressure and heat drop is known so the direction of the flows is deduced. Then, the temperature of the original flow and its partial pressures $[T, P_i]$ can be known from upstream T and P_i.

Then equations (17) to (21) are used. For equations (18) to (21), T_{C2} must be replaced by the temperature of the upstream, and the partial pressures are also given by the upstream capacitance element.

Gates are symbolized by MR elements, controlled by squared signals. It is the R_{output} described in equation (22), where D_g is controlled ($0 < D_g < D$).

The abatement rate *y(t)* is measured by adding the pollutant molar fractions at the exits of MR_{valve} and MR_{valve}*

$$y(t) = 1 - \frac{x_{C_3H_8,valve}(t)+x_{C_3H_8,valve^*}(t)}{x_{C_3H_8,inlet}(t)+x_{C_3H_8,inlet*}(t)} \quad (53)$$

5. SIMULATION RESULTS

5.1. Comparison of the BG Model with the Literature

The reverse-flow operating mode was compared to V. Balcaen (2011) detailed simulation, showing the temperature spacial distribution in a reverse flow reactor in quasi-steady state.

The reactor dimensions and materials are given in Table 3. The experiment starts with a hot monolith at a homogenous temperature of 725K. Then, an air flow of $1.436*10^{-6}$ kg/s/channel is introduced at T=300K, x_{C3H8}=0.0035, x_{O2} = 0.21, x_{N2}=0.78, x_{H2O} = x_{CO2} = 0.

The comparison model results are represented by the dotted curve, the simulation results of the current model by the continuous line.

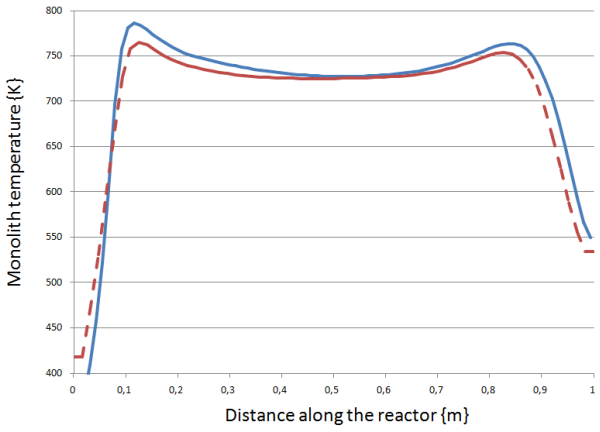

Figure 6: comparison with previous work (250s after the 8th semi-cycle)

Balcaen results are based on Heynderickx (2010) kinetic model whereas the bond graph calculations are

based on Ramanathan's approximation. Moreover, Balcaen simulation was run with a 64 sections model.

The current model presents a difference of about 5% with Balcaen's one which is satisfying.

In Balcaen 's thesis, no transient state investigations were presented.

5.2. Some Case Studies

1. Reactor simulation under standard conditions:

The reactor starts-up with an initial monolith temperature of 300K. The air flow is introduced with a pollutant concentration of 3500 ppmv and a temperature of 300K.

The central part of the reactor [0.384-0.616m] is warmed-up by an external heat source. The heater is constituted of several independent sub-systems with a closed-loop control, each cell beneficiates of one sub-system and its control.

The closed loop system has a set point of 600K, and cannot supply more power than 10W/channel. An hysteresis with amplitude of 50K is added to prevent small oscillations.

On Figure 7 the power delivered by the heater, the abatement rate and the temperature of a middle section are reported.

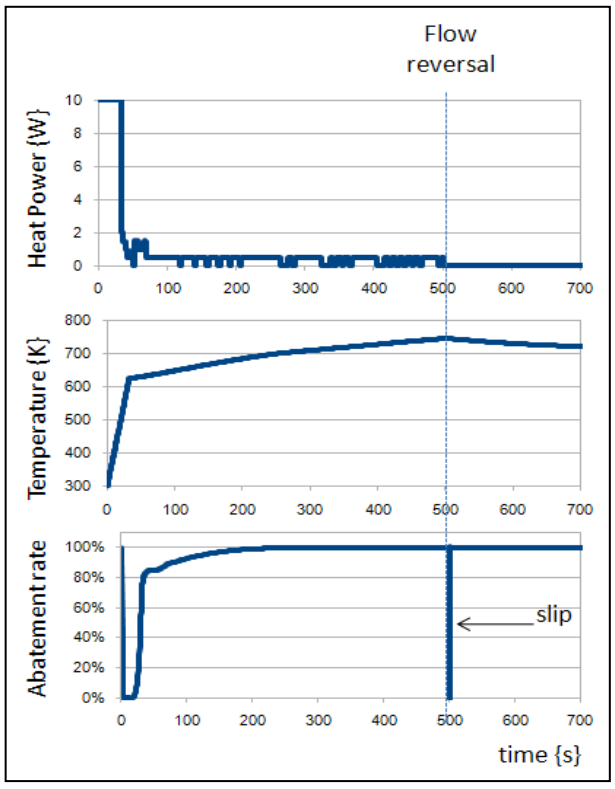

Figure 7: Heater Power, Abatement Rate and Temperature versus Time

In the current study, the whole heating-step occurs during the first semi-cycle.

After about 50 s the system is very close to the set point temperature. However, the temperature continues to increase as a consequence of the heat released by the combustion.

The small amounts of power released during the first semi-cycle are liberated by the upstream cell's heater. Indeed, this cell is directly in contact with cold cells and receives fresh air (at a temperature close to 300K). Hence, it dissipates a lot of heat and requires more power than downstream cells. The advantage of RFR is here demonstrated because for the time interval 400-500s, the set-up dissipates 0.25W/channel which means about 21kW for an industrial installation of 100L/s, 504KWh/day ; when the flow is reversed, the energetic consumptions drops to zero.

Just before the first semi-cycle ends-up, the downstream part of the reactor is hot, while the upstream remains cold.

When the flow is reversed, the autothermal process starts: the air is warmed-up by the hot sections ignites and liberates heat in the cold sections.

During the flow reversal, the abatement rate falls to zero. It is due to the pollutant repartition within the channel just before the flow reversal (see Figure 8).

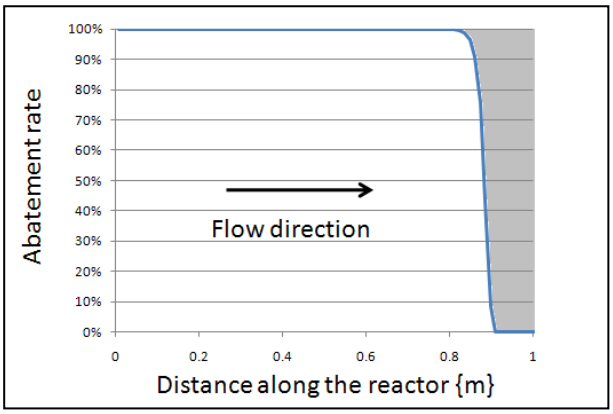

Figure 8: Pollutant Concentration Profile just after Flow Reversal (16th flow reversal)

A few amount of pollutant remains in the cold part of the reactor (here on the right). Usually, the air flow ensures the pollutant is going to cross the reactor and burn. However, during the flow reversal, the pollutant is ejected and does not pass through the channel. All this fresh and polluted air is liberated. This is an important phenomenon in the study of reverse-flow reactors, as it will be shown in the next case.

2. Influence of the switching time

To check the influence of the switching time on transient and pseudo steady-state reactor behavior, a simulation scenario was designed.

The reactor starts with an homogenous monolith temperature T=500K, and polluted air is introduced under standard conditions (3500ppmv, 300K).

Several semi-cycle times are tested (tsc = 50 s, 500 s, 5000 s).

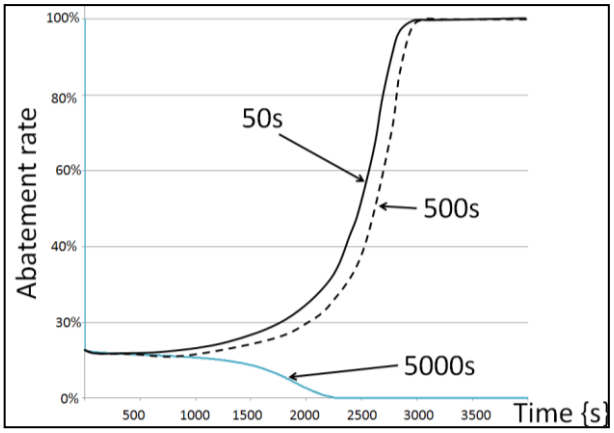

Figure 9: Abatement Rate versus Time for several Semi-Cycle Times

The ignition process occurs in the time interval 0 to 3000 s. The abatement rate shows this process mostly depends on physical parameters of the reactor. After 1000 s, the 5000 s semi-cycle time reactor starts loosing ignition. An interpretation is if the switching time is too high (tsc=5000s), the reaction front quits the channel, and the pollutant abatement goes down to zero. The transient state is shorter of about 100s for short semi-cycle time. As a result, the cumulative pollutant emissions are lower of 6% at t=4000s.

However if the switching time is too short, slips emissions rise-up. Figure 10 below shows the abatement rate and the slip emission around t=17500s. Slip emission is defined as :

$$slip\_emissions = \frac{\int_{To}^{t} \dot{n}_{C3H8}\, dt}{\int_{17250}^{17750} \dot{n}_{C3H8} dt} \quad (54)$$

$$studied\_case$$

$$tsc=500s$$

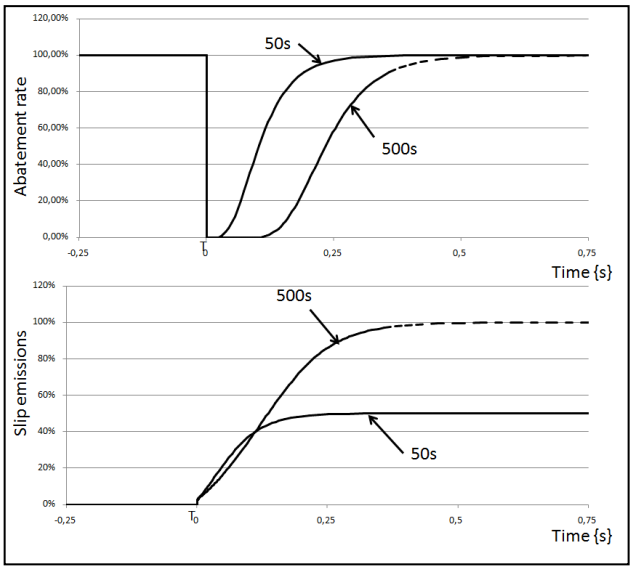

Figure 10: Abatement Rate and Slip Emissions for 50s and 500s Semi-Cycle Times at T_0=17500s Flow Reversal

The amplitude of the emissions of the slip in the case of t_{sc} = 50s is about half of the amplitude for t_{sc}=500s, because the penetration of the heat-front is deeper in the 500s case. However, the flow is reversed 10 times more frequently in the case of t_{sc} = 50s and hence, during 500s the t_{sc} = 50s reactor emits 5 times more pollutant in the atmosphere. As a result, it is preferable to work on large semi-cycle time during the steady state. However, according to Figure 9 it is worth to start-up with short semi-cycle time. Thus, this study shows the interest of a dynamic variation of switching time frequency during the reactor start-up.

6. CONCLUSION AND FUTURE WORKS

In this paper, a bond graph model for monolithic reverse-flow reactors has been developed. Its results match with previous studies on this subject.
On the one hand, simulations of an 82 cells model were run with a ratio of about 10s of simulation per second of calculation on a laptop. This rate can clearly be improved by, for instance, simplifying the reaction rate expression or reducing the number of cells through a variable space-step computation.
On the other hand, the reverse-flow reactor can be handled through several parameters like purge time, mass-flow rate or heat exchange in the monolith.
Hence, supervision strategy field is opened for monolithic reverse-flow-reactor. Moreover, the bond-graph permits to simulate this end-of pipe device as a part of a bigger system.
Future works will study critical conditions of use under dynamic constraints like a dynamic variation of pollutant concentration or inlet mass-flow rate fluctuation.

APPENDIX

Table 3: standard values of parameters

Solver : Vode& Adams	Step size absolute precision relative precision	0.001 10^{-8} 10^{-8}
Length of the reactor	L {m}	1.000
Geometry of the channel : circular	Nu Sh	4.364 4.364
Length of inert section	$L_g = 0.05 * L$ {m}	0.05
Hydraulic diameter of one channel	D {m}	0.002
Number of channels	Nchannel	100
Number of cells	N	82
Thickness of the washcoat	tw {mm}	25
Thickness of the monolith	tm {mm}	150
Thickness of the insulation	ti {mm}	1

Thermal conductivity of the insulation	λ_i {W/m.K}	0.002
density of the catalyst	ρ_c {kg/m^3}	4000
Porosity of the washcoat	ε	0.5
Density of the monolith	ρ_m {kg/m^3}	8000
Thermal conductivity of the air ($\lambda = \lambda_a*T+\lambda_b$)	λ {W/m.K}	$\lambda_a = 5.91*10^{-5}$ $\lambda_b = 0.01$
Diffusivity of the air ($\alpha = \alpha_a*T + \alpha_b$)	α {m²/s}	$\alpha_a = 2.08*10^{-7}$ $\alpha_b = -4.56*10^{-5}$
Viscosity of the air ($\mu = \mu_a*T + \mu_b$)	μ {Pa.s}	$\mu_a = 3.30*10^{-8}$ $\mu_a = 3.30e^{-8}$
Heat capacity of the air	Cp {J/mol.K}	29.1
Thermal conductivity of the washcoat	λ_w {W/m.K}	16
Heat capacity of the catalyst	Cc { J/kg.K}	947
Thermal conductivity of the monolith	λ_m {W/m.K}	16
Heat capacity of the monolith	Cm {J/kg.K}	502
Reaction enthalpy	ΔrH {J/mol}	- 2040240*10^3
Frequency rate of the reaction	Ar {s^{-1}}	9.6*10^{10}
Reaction activation energy	E {J/mol}	89791
Semi-cycle time	t_{sc} {s}	500s
Atmospheric pressure	P_0 {Pa}	101325
Inlet temperature	T_{in} {K}	300

NOTATIONS:

Q_v: Volume flow rate
h: Newton's heat transfer coefficient
β: Fick's heat transfer coefficient
$q_{m,in}$: Mass flow rate
M: Molecular weight
P_i: Partial pressure in specie i
$x_{i,in}$: Inlet molar fraction of specie i
τ: Specific time of reactor thermal behavior
η: Thiele factor
θ: non-dimensional number for Thiele factor
r_v: volumetric reaction rate
Layers :

- ms : main-stream
- w : washcoat (catalyst+air bubbles)
- m : monolith
- i : insulation
- c : catalyst

REFERENCES

Balcaen, V., 2011. The Total Oxidation of Propane over Metal Oxyde Catalyst: Transient Kinetics and Monolith Reactors, Thesis (PhD). Gent University.

Couenne, F., Jallut, C., Maschke, B., Breedveld, P. C., Tayakout, M., 2006. Bond Graph modeling for chemical reactors. *Mathematical and Computer Modeling of Dynamical Systems*, 12, 159.

Heny, C., Simanca, D., Delgado, M., 2006. Pseudo-bond graph model and simulation of a continuous stirred tank reactor. *Journal of the Franklin Institute*, 12, 159.

Heynderickx, M.P., Thybaut J.W., Poelman, H., Poelman, D., Marin, G.B., 2010. Kinetic modeling of the total oxidation of propane over CuO-CeO_2/γ-Al_2O_3. *Applied Catalysis B: Environmental*, 95, 26-38.

Karnopp, D., 1990. Bond graph models for electrochemical energy storage : electrical, chemical and thermal effects. *Journal of the Franklin Institute*, 327(6), 983-992.

MacKenzie, S.A., Gawthrop, P.J., Jones, R.W., 1993. Modeling chemical process with pseudo bond graphs. *Proceedings of the International Conference in Bond Graph Modeling*, pp. 327-332. January 17-20, La Jolla (California, USA).

Matros, Y.S., Bunimovich, G.A., 1996. Reverse-flow operation in fixed bed catalytic reactors. *Catalysis Reviews: Science and Engineering*, 38(1), 1-68.

Marin, P., Ordonez, S., Diez, F.V., 1990. Simplified design methods of reverse-flow catalytic combustors for the treatment of lean hydrocarbon-air mixtures. *Chemical Engineering and Processing*, 48, 229-238.

Ramanathan, K., West, D.H., Balakotaiah, V., 2004. Optimal design of catalytic converters for minimizing cold-start emissions. *Catalysis Today*, *98*, 357–373

Ramdani, K., Pontier, R., Schweich, D., 2001. Reverse flow reactor at short switching periods for VOC combustion. *Chemical Engineering Science*, 56(4), 1531-1539

Thoma, J. and Ould-Bouamama, B., 1999. Modeling and Simulation in Thermal and Chemical Engineering. London: Pringer Engineering Edition.

Van de Beld, B., Westerterp, KR., 1994a. Air purification by catalytci oxidation in a reactor with periodic reverse flow. *Chemical Engineering & Technology*, 17, 217-226

Van de Beld, B., Borman, R.A., Derkx, O.R., van Woezik, B.A.A., Westerterp, K.R., 1994b. Removal of volatile organic compounds from polluted air in a reverse flow reactor: An experimental study. *Industrial and Engineering Chemistry Research*, 33, 2946-2956